DESY-01-216
December 2001

arXiv:hep-ex/0202034v1 19 Feb 2002

Measurement of the photon-proton total cross section at a center-of-mass energy of 209 GeV at HERA

ZEUS Collaboration

Abstract

The photon-proton total cross section has been measured in the process $e^+p \to e^+\gamma p \to e^+X$ with the ZEUS detector at HERA. Events were collected with photon virtuality $Q^2 < 0.02$ GeV^2 and average γp center-of-mass energy $W_{\gamma p} = 209$ GeV in a dedicated run, designed to control systematic effects, with an integrated luminosity of 49 nb^{-1}. The measured total cross section is $\sigma_{\rm tot}^{\gamma p} = 174 \pm 1({\rm stat.}) \pm 13({\rm syst.})$ μb. The energy dependence of the cross section is compatible with parameterizations of high-energy pp and $p\bar{p}$ data.

The ZEUS Collaboration

S. Chekanov, M. Derrick, D. Krakauer, S. Magill, B. Musgrave, A. Pellegrino, J. Repond, R. Yoshida
Argonne National Laboratory, Argonne, Illinois 60439-4815 [n]

M.C.K. Mattingly
Andrews University, Berrien Springs, Michigan 49104-0380

P. Antonioli, G. Bari, M. Basile, L. Bellagamba, D. Boscherini, A. Bruni, G. Bruni, G. Cara Romeo, L. Cifarelli, F. Cindolo, A. Contin, M. Corradi, S. De Pasquale, P. Giusti, G. Iacobucci, G. Levi, A. Margotti, T. Massam, R. Nania, F. Palmonari, A. Pesci, G. Sartorelli, A. Zichichi
University and INFN Bologna, Bologna, Italy [e]

G. Aghuzumtsyan, D. Bartsch, I. Brock, J. Crittenden[1], S. Goers, H. Hartmann, E. Hilger, P. Irrgang,
H.-P. Jakob, A. Kappes, U.F. Katz[2], R. Kerger, O. Kind, E. Paul, J. Rautenberg[3], R. Renner, H. Schnurbusch, A. Stifutkin, J. Tandler, K.C. Voss, A. Weber, H. Wessoleck
Physikalisches Institut der Universität Bonn, Bonn, Germany [b]

D.S. Bailey[4], N.H. Brook[4], J.E. Cole, B. Foster, G.P. Heath, H.F. Heath, S. Robins, E. Rodrigues[5], J. Scott, R.J. Tapper, M. Wing
H.H. Wills Physics Laboratory, University of Bristol, Bristol, United Kingdom [m]

M. Capua, A. Mastroberardino, M. Schioppa, G. Susinno
Calabria University, Physics Department and INFN, Cosenza, Italy [e]

H.Y. Jeoung, J.Y. Kim, J.H. Lee, I.T. Lim, K.J. Ma, M.Y. Pac[6]
Chonnam National University, Kwangju, Korea [g]

A. Caldwell, M. Helbich, X. Liu, B. Mellado, S. Paganis, W.B. Schmidke, F. Sciulli
Nevis Laboratories, Columbia University, Irvington on Hudson, New York 10027 [o]

J. Chwastowski, A. Eskreys, J. Figiel, K. Olkiewicz, M.B. Przybycień[7], P. Stopa, L. Zawiejski
Institute of Nuclear Physics, Cracow, Poland [i]

B. Bednarek, I. Grabowska-Bold, K. Jeleń, D. Kisielewska, A.M. Kowal[8], M. Kowal, T. Kowalski, B. Mindur, M. Przybycień, E. Rulikowska-Zarębska, L. Suszycki, D. Szuba, J. Szuba[9]
Faculty of Physics and Nuclear Techniques, University of Mining and Metallurgy, Cracow, Poland [i]

A. Kotański, W. Słomiński[10]
Department of Physics, Jagellonian University, Cracow, Poland

L.A.T. Bauerdick[11], U. Behrens, K. Borras, V. Chiochia, D. Dannheim, K. Desler[12], G. Drews, J. Fourletova, A. Fox-Murphy, U. Fricke, A. Geiser, F. Goebel, P. Göttlicher, R. Graciani, T. Haas, W. Hain, G.F. Hartner, S. Hillert, U. Kötz, H. Kowalski, H. Labes, D. Lelas, B. Löhr, R. Mankel, J. Martens[13], M. Martínez[11], M. Moritz, D. Notz, M.C. Petrucci, A. Polini, U. Schneekloth, F. Selonke, S. Stonjek, B. Surrow[14], J.J. Whitmore[15], R. Wichmann[16], G. Wolf, C. Youngman, W. Zeuner
Deutsches Elektronen-Synchrotron DESY, Hamburg, Germany

C. Coldewey[17], A. Lopez-Duran Viani, A. Meyer, S. Schlenstedt
DESY Zeuthen, Zeuthen, Germany

G. Barbagli, E. Gallo, C. Genta, P. G. Pelfer
University and INFN, Florence, Italy [e]

A. Bamberger, A. Benen, N. Coppola, P. Markun, H. Raach, S. Wölfle
Fakultät für Physik der Universität Freiburg i.Br., Freiburg i.Br., Germany [b]

M. Bell, P.J. Bussey, A.T. Doyle, C. Glasman, S. Hanlon, S.W. Lee, A. Lupi, G.J. McCance, D.H. Saxon, I.O. Skillicorn
Department of Physics and Astronomy, University of Glasgow, Glasgow, United Kingdom [m]

B. Bodmann, U. Holm, H. Salehi, K. Wick, A. Ziegler, Ar. Ziegler
Hamburg University, I. Institute of Exp. Physics, Hamburg, Germany [b]

T. Carli, I. Gialas[18], K. Klimek, E. Lohrmann, M. Milite
Hamburg University, II. Institute of Exp. Physics, Hamburg, Germany [b]

C. Collins-Tooth, C. Foudas, R. Gonçalo[5], K.R. Long, F. Metlica, D.B. Miller, A.D. Tapper, R. Walker
Imperial College London, High Energy Nuclear Physics Group, London, United Kingdom [m]

P. Cloth, D. Filges
Forschungszentrum Jülich, Institut für Kernphysik, Jülich, Germany

M. Kuze, K. Nagano, K. Tokushuku[19], S. Yamada, Y. Yamazaki
Institute of Particle and Nuclear Studies, KEK, Tsukuba, Japan [f]

A.N. Barakbaev, E.G. Boos, N.S. Pokrovskiy, B.O. Zhautykov
Institute of Physics and Technology of Ministry of Education and Science of Kazakhstan, Almaty, Kazakhstan

S.H. Ahn, S.B. Lee, S.K. Park
Korea University, Seoul, Korea [g]

H. Lim, D. Son
Kyungpook National University, Taegu, Korea [g]

F. Barreiro, G. García, O. González, L. Labarga, J. del Peso, I. Redondo[20], J. Terrón, M. Vázquez
Departameto de Física Teórica, Universidad Autónoma Madrid, Madrid, Spain [l]

M. Barbi, A. Bertolin, F. Corriveau, A. Ochs, S. Padhi, D.G. Stairs, M. St-Laurent
Department of Physics, McGill University, Montréal, Québec, Canada H3A 2T8 [a]

T. Tsurugai
Meiji Gakuin University, Faculty of General Education, Yokohama, Japan

A. Antonov, V. Bashkirov[21], P. Danilov, B.A. Dolgoshein, D. Gladkov, V. Sosnovtsev, S. Suchkov
Moscow Engineering Physics Institute, Moscow, Russia [j]

R.K. Dementiev, P.F. Ermolov, Yu.A. Golubkov, I.I. Katkov, L.A. Khein, N.A. Korotkova, I.A. Korzhavina, V.A. Kuzmin, B.B. Levchenko, O.Yu. Lukina, A.S. Proskuryakov, L.M. Shcheglova, A.N. Solomin, N.N. Vlasov, S.A. Zotkin
Moscow State University, Institute of Nuclear Physics, Moscow, Russia [k]

C. Bokel, J. Engelen, S. Grijpink, E. Koffeman, P. Kooijman, E. Maddox, S. Schagen, E. Tassi, H. Tiecke, N. Tuning, J.J. Velthuis, L. Wiggers, E. de Wolf
NIKHEF and University of Amsterdam, Amsterdam, Netherlands [h]

N. Brümmer, B. Bylsma, L.S. Durkin, J. Gilmore, C.M. Ginsburg, C.L. Kim, T.Y. Ling
Physics Department, Ohio State University, Columbus, Ohio 43210 [n]

S. Boogert, A.M. Cooper-Sarkar, R.C.E. Devenish, J. Ferrando, T. Matsushita, M. Rigby, O. Ruske[22], M.R. Sutton, R. Walczak
Department of Physics, University of Oxford, Oxford United Kingdom [m]

R. Brugnera, R. Carlin, F. Dal Corso, S. Dusini, A. Garfagnini, S. Limentani, A. Longhin, A. Parenti, M. Posocco, L. Stanco, M. Turcato
Dipartimento di Fisica dell' Università and INFN, Padova, Italy [e]

L. Adamczyk[23], B.Y. Oh, P.R.B. Saull[23]
Department of Physics, Pennsylvania State University, University Park, Pennsylvania 16802 [o]

Y. Iga
Polytechnic University, Sagamihara, Japan [f]

G. D'Agostini, G. Marini, A. Nigro
Dipartimento di Fisica, Università 'La Sapienza' and INFN, Rome, Italy [e]

C. Cormack, J.C. Hart, N.A. McCubbin
Rutherford Appleton Laboratory, Chilton, Didcot, Oxon, United Kingdom [m]

C. Heusch
University of California, Santa Cruz, California 95064 [n]

I.H. Park
Seoul National University, Seoul, Korea

N. Pavel
Fachbereich Physik der Universität-Gesamthochschule Siegen, Germany

H. Abramowicz, S. Dagan, A. Gabareen, S. Kananov, A. Kreisel, A. Levy
Raymond and Beverly Sackler Faculty of Exact Sciences, School of Physics, Tel-Aviv University, Tel-Aviv, Israel [d]

T. Abe, T. Fusayasu, T. Kohno, K. Umemori, T. Yamashita
Department of Physics, University of Tokyo, Tokyo, Japan [f]

R. Hamatsu, T. Hirose, M. Inuzuka, S. Kitamura[24], K. Matsuzawa, T. Nishimura
Tokyo Metropolitan University, Deptartment of Physics, Tokyo, Japan [f]

M. Arneodo[25], N. Cartiglia, R. Cirio, M. Costa, M.I. Ferrero, S. Maselli, V. Monaco, C. Peroni, M. Ruspa, R. Sacchi, A. Solano, A. Staiano
Università di Torino, Dipartimento di Fisica Sperimentale and INFN, Torino, Italy [e]

R. Galea, T. Koop, G.M. Levman, J.F. Martin, A. Mirea, A. Sabetfakhri
Department of Physics, University of Toronto, Toronto, Ontario, Canada M5S 1A7 [a]

J.M. Butterworth, C. Gwenlan, R. Hall-Wilton, M.E. Hayes[26], E.A. Heaphy, T.W. Jones, J.B. Lane, M.S. Lightwood, B.J. West
Physics and Astronomy Department, University College London, London, United Kingdom [m]

J. Ciborowski[27], R. Ciesielski, G. Grzelak, R.J. Nowak, J.M. Pawlak, B. Smalska[28], J. Sztuk[29], T. Tymieniecka[30], A. Ukleja[30], J. Ukleja, J.A. Zakrzewski, A.F. Żarnecki
Warsaw University, Institute of Experimental Physics, Warsaw, Poland [i]

M. Adamus, P. Plucinski
Institute for Nuclear Studies, Warsaw, Poland [i]

Y. Eisenberg, L.K. Gladilin[31], D. Hochman, U. Karshon
Department of Particle Physics, Weizmann Institute, Rehovot, Israel [c]

J. Breitweg[32], D. Chapin, R. Cross, D. Kçira, S. Lammers, D.D. Reeder, A.A. Savin, W.H. Smith
Department of Physics, University of Wisconsin, Madison, Wisconsin 53706 [n]

A. Deshpande, S. Dhawan, V.W. Hughes, P.B. Straub
Department of Physics, Yale University, New Haven, Connecticut 06520-8121 [n]

S. Bhadra, C.D. Catterall, S. Fourletov, S. Menary, M. Soares, J. Standage
Department of Physics, York University, Ontario, Canada M3J 1P3 [a]

[1] now at Cornell University, Ithaca, USA
[2] on leave of absence at University of Erlangen-Nürnberg, Germany
[3] supported by the GIF, contract I-523-13.7/97
[4] PPARC Advanced fellow
[5] supported by the Portuguese Foundation for Science and Technology (FCT)
[6] now at Dongshin University, Naju, Korea
[7] now at Northwestern Univ., Evaston/IL, USA
[8] supported by the Polish State Committee for Scientific Research, grant no. 5 P-03B 13720
[9] partly supported by the Israel Science Foundation and the Israel Ministry of Science
[10] Department of Computer Science, Jagellonian University, Cracow
[11] now at Fermilab, Batavia/IL, USA
[12] now at DESY group MPY
[13] now at Philips Semiconductors Hamburg, Germany
[14] now at Brookhaven National Lab., Upton/NY, USA
[15] on leave from Penn State University, USA
[16] now at Mobilcom AG, Rendsburg-Büdelsdorf, Germany
[17] now at GFN Training GmbH, Hamburg
[18] Univ. of the Aegean, Greece
[19] also at University of Tokyo
[20] supported by the Comunidad Autonoma de Madrid
[21] now at Loma Linda University, Loma Linda, CA, USA
[22] now at IBM Global Services, Frankfurt/Main, Germany
[23] partly supported by Tel Aviv University
[24] present address: Tokyo Metropolitan University of Health Sciences, Tokyo 116-8551, Japan
[25] also at Università del Piemonte Orientale, Novara, Italy
[26] now at CERN, Geneva, Switzerland
[27] also at Łódź University, Poland
[28] supported by the Polish State Committee for Scientific Research, grant no. 2 P-03B 00219
[29] Łódź University, Poland
[30] sup. by Pol. State Com. for Scien. Res., 5 P-03B 09820 and by Germ. Fed. Min. for Edu. and Research (BMBF), POL 01/043
[31] on leave from MSU, partly supported by University of Wisconsin via the U.S.-Israel BSF
[32] now at EssNet Deutschland GmbH, Hamburg, Germany

[a] supported by the Natural Sciences and Engineering Research Council of Canada (NSERC)
[b] supported by the German Federal Ministry for Education and Research (BMBF), under contract numbers HZ1GUA 2, HZ1GUB 0, HZ1PDA 5, HZ1VFA 5
[c] supported by the MINERVA Gesellschaft für Forschung GmbH, the Israel Science Foundation, the U.S.-Israel Binational Science Foundation, the Israel Ministry of Science and the Benozyio Center for High Energy Physics
[d] supported by the German-Israeli Foundation, the Israel Science Foundation, and by the Israel Ministry of Science
[e] supported by the Italian National Institute for Nuclear Physics (INFN)
[f] supported by the Japanese Ministry of Education, Science and Culture (the Monbusho) and its grants for Scientific Research
[g] supported by the Korean Ministry of Education and Korea Science and Engineering Foundation
[h] supported by the Netherlands Foundation for Research on Matter (FOM)
[i] supported by the Polish State Committee for Scientific Research, grant no. 115/E-343/SPUB-M/DESY/P-03/DZ 121/2001-2002
[j] partially supported by the German Federal Ministry for Education and Research (BMBF)
[k] supported by the Fund for Fundamental Research of Russian Ministry for Science and Education and by the German Federal Ministry for Education and Research (BMBF)
[l] supported by the Spanish Ministry of Education and Science through funds provided by CICYT
[m] supported by the Particle Physics and Astronomy Research Council, UK
[n] supported by the US Department of Energy
[o] supported by the US National Science Foundation

1 Introduction

A measurement of the photon-proton total hadronic cross section at the high center-of-mass energy of the HERA ep collider provides a test of the asymptotic behavior of total cross sections. The energy dependences of the pp, $\bar{p}p$, Kp and πp total cross sections are successfully parameterized by the exchanges of Regge trajectories [1]. Phenomenological fits [2–5] based on Regge theory are able to describe all the hadronic total cross sections in the full energy range using the form

$$\sigma_{\rm tot} = A \cdot s^{\epsilon} + B \cdot s^{-\eta}, \tag{1}$$

where s is the square of the center-of-mass energy and A and B are constants. The parameters $\alpha_{I\!P}(0) = 1 + \epsilon$ and $\alpha_{I\!R}(0) = 1 - \eta \approx 0.55$ denote the intercepts of the Pomeron and Reggeon trajectories, respectively. At the highest energies, the Pomeron intercept describes the weak energy dependence of hadronic total cross sections by the form $\sigma_{\rm tot} \propto s^{\epsilon}$, where $0.08 < \epsilon < 0.096$ [2–5].

The soft hadronic behavior of the photon is well described by the vector-meson dominance model (VDM) [6, 7], in which the photon is considered to be a superposition of the light vector mesons (ρ^0, ω and ϕ), which interact with the proton. This model has been well tested at low energies [8]. If, at asymptotic energies, the photon can be entirely described by the VDM, the same universal energy dependence is expected for the hadron-proton and photon-proton total cross sections. Furthermore, if these total cross sections are dominated by the exchange of a Pomeron trajectory at high energies, the pp, γp and $\gamma\gamma$ total cross sections will be related.

This paper reports a new ZEUS measurement of the photon-proton total cross section, using the reaction $e^+p \to e^+\gamma p \to e^+X$. The energy of the scattered positron was measured, thus providing a determination of the photon energy; the limited angular acceptance for the scattered positron restricted the virtuality of the tagged photon to very small values, $Q^2 < 0.02\,{\rm GeV}^2$. This measurement requires the accurate determination of the acceptance of the positron-tagging calorimeter. For this reason, the experiment was performed under closely controlled conditions of the positron-beam parameters, resulting in a reduction of systematic effects. The detector acceptance for the hadronic final-state X in the above reaction is sensitive to the topologies and relative fractions of the photoproduction subprocesses. For the previous ZEUS measurements [9], the subprocess cross sections were extracted through fits to the distribution of the energy deposits in the main ZEUS calorimeter. Detailed studies of several of the subprocesses have subsequently been published by ZEUS [10–14], permitting improved estimates of the respective cross sections. In the present paper, these subprocess measurements are used as constraints to obtain a more accurate measurement of the photoproduction total cross section than was previously possible. Because of these improvements, the results of this paper supersede those of the previous publications [9]. The photon-proton total cross section has also been measured at a similar center-of-mass energy by the H1 Collaboration [15].

2 Kinematics

The photon-proton total cross section has been measured in the process $e^+p \to e^+\gamma p \to e^+X$, where the interacting photon is almost real. The event kinematics may be described in terms

of Lorentz-invariant variables: the photon virtuality, Q^2, and the event inelasticity, y, defined by

$$Q^2 = -q^2 = -(k - k')^2$$

and

$$y = \frac{p \cdot q}{p \cdot k}\,,$$

where k, k' and p are the four-momenta of the incoming positron, scattered positron and incident proton, respectively. The square of the photon-proton center-of-mass energy is given by

$$W^2_{\gamma p} = (q + p)^2\,.$$

These variables can be expressed in terms of the experimentally measured quantity E'_e using

$$Q^2 = Q^2_{\rm min} + 4E_e E'_e \sin^2\frac{\vartheta}{2}\,,$$

$$y = 1 - \frac{E'_e}{E_e}\cos^2\frac{\vartheta}{2} \simeq 1 - \frac{E'_e}{E_e}\,,$$

$$W_{\gamma p} = 2\sqrt{E_e E_p y}\,,$$

where

$$Q^2_{\rm min} = \frac{m_e^2 y^2}{1-y}\,,$$

E_e, E'_e and E_p are the energies of the incoming positron, scattered positron and incident proton, respectively, ϑ is the positron scattering angle with respect to the initial positron direction and m_e is the positron mass. The scattered positron was recorded in a positron tagger close to the beam line, restricting the production angle, ϑ (and hence Q^2), to small values. The photon virtuality ranged from the kinematic minimum, $Q^2_{\rm min} \simeq 10^{-7}$ GeV^2, up to $Q^2_{\rm max} \simeq 0.02$ GeV^2, given by the acceptance of the positron tagger. The median Q^2 is about 5×10^{-5} GeV^2.

The equivalent photon approximation [16] relates the electroproduction cross section to a photoproduction cross section. The double-differential ep cross section can be written as

$$\frac{d^2\sigma^{ep}_{\rm tot}(y,Q^2)}{dydQ^2} = \frac{\alpha}{2\pi}\frac{1}{Q^2}\left[\left(\frac{1+(1-y)^2}{y} - \frac{2(1-y)}{y}\frac{Q^2_{\rm min}}{Q^2}\right)\cdot\sigma^{\gamma p}_T(y,Q^2) + \frac{2(1-y)}{y}\cdot\sigma^{\gamma p}_L(y,Q^2)\right]\,, \qquad (2)$$

where $\sigma^{\gamma p}_T$ is the cross section for interactions between the proton and a photon with transverse polarization, and $\sigma^{\gamma p}_L$ is the cross section for interactions with longitudinally polarized photons. The longitudinal cross section is expected to be small ($\sigma^{\gamma p}_L/\sigma^{\gamma p}_T < 0.1\%$ [17]), and has been ignored, as has the Q^2 dependence of $\sigma^{\gamma p}_T$ (<0.1% in the range of Q^2 of this measurement [6,7]).

Integrating Eq. (2) over Q^2 gives the single ep differential cross section in terms of the γp total cross section:

$$\frac{d\sigma^{ep}_{\rm tot}(y)}{dy} = \frac{\alpha}{2\pi}\left[\frac{1+(1-y)^2}{y}\ln\frac{Q^2_{\rm max}}{Q^2_{\rm min}} - \frac{2(1-y)}{y}\left(1 - \frac{Q^2_{\rm min}}{Q^2_{\rm max}}\right)\right]\sigma^{\gamma p}_{\rm tot}(y) = F_\gamma(y)\sigma^{\gamma p}_{\rm tot}(y)\,. \qquad (3)$$

Integrating Eq. (3) between y_1 and y_2, and neglecting the weak y-dependence of $\sigma_{\rm tot}^{\gamma p}(y)$ in the integral, the electroproduction cross section is

$$\sigma_{\rm tot}^{ep} = \int_{y_1}^{y_2} F_\gamma(y)\sigma_{\rm tot}^{\gamma p}(y)\, dy = f_\gamma \sigma_{\rm tot}^{\gamma p}\,,$$

where

$$f_\gamma = \int_{y_1}^{y_2} F_\gamma(y) dy\,, \tag{4}$$

and $y_1 = 0.42$ and $y_2 = 0.56$ are derived from the minimum and maximum detected positron energies, respectively (see Section 3).

3 Experimental conditions

The data were taken with the ZEUS detector during a dedicated run in 1996, when HERA collided 820 GeV protons with 27.5 GeV positrons. The proton and positron beams each contained 177 colliding bunches, together with 3 additional unpaired proton and 31 unpaired positron bunches. These additional bunches were used for background studies. The time between bunch crossings was 96 ns.

The ZEUS detector has been described in detail elsewhere [18]. Most important for this measurement are the uranium-scintillator sampling calorimeter (CAL) [19], the central tracking detector (CTD) [20] and two lead-scintillator calorimeters close to the e^+ beampipe at $Z = -107$ m (photon tagger) and $Z = -35$ m (positron or "35m" tagger) [21]. The CAL is separated into three parts, forward[1] (FCAL, $2.6^\circ < \theta < 36.7^\circ$), barrel (BCAL, $36.7^\circ < \theta < 129.1^\circ$), and rear (RCAL, $129.1^\circ < \theta < 176.2^\circ$). Each CAL part is longitudinally segmented into electromagnetic (EMC) and hadronic (HAC) sections. Each section is further subdivided transversely into cells of typically 5×20 cm^2 (10×20 cm^2 in RCAL) for the EMC and 20×20 cm^2 for the HAC sections. The total number of CAL cells is 5918. The CAL relative energy resolution for electromagnetic showers is $\sigma_E/E \simeq 0.18/\sqrt{E(\mathrm{GeV})}$ and for hadronic showers is $\sigma_E/E \simeq 0.35/\sqrt{E(\mathrm{GeV})}$ under test-beam conditions. The CAL also provides timing information, with a resolution of 1 ns for energy deposits greater than 4.5 GeV. The CTD operates in a 1.43 T solenoidal magnetic field, and has a relative transverse-momentum resolution for full-length tracks of $\sigma_{p_T}/p_T = 0.0058\, p_T \oplus 0.0065 \oplus 0.0014/p_T$, with p_T measured in GeV. The photon-tagger relative energy resolution is $\sigma_E/E = 0.23/\sqrt{E(\mathrm{GeV})}$, and the 35m-tagger relative energy resolution is $\sigma_E/E = 0.19/\sqrt{E(\mathrm{GeV})}$. Both the photon tagger and the 35m tagger are also equipped with shower-position detectors. These consist of both horizontal and vertical scintillator strips providing a position resolution of 0.3 cm in both X and Y.

[1] The ZEUS coordinate system is a right-handed Cartesian system, with the Z axis pointing in the proton beam direction, referred to as the "forward direction", and the X axis pointing left towards the center of HERA. The coordinate origin is at the nominal interaction point. The pseudorapidity is defined as $\eta = -\ln\left(\tan\frac{\theta}{2}\right)$, where the polar angle, θ, is measured with respect to the proton beam direction. The azimuthal angle is denoted by ϕ.

The luminosity was measured via the Bethe-Heitler bremsstrahlung process $ep \to e\gamma p$, using the photon tagger [21], which detects photons with scattering angles smaller than $\vartheta = 180^\circ - \theta = 0.54$ mrad. The accumulated luminosity used for this measurement was 49.26 ± 0.54 (syst.) nb^{-1}.

For this measurement, the hadronic final-state X was detected in the main ZEUS detector and the final-state positrons were tagged in the 35m tagger after traversing a window in the beam pipe. The geometric acceptance of the 35m tagger restricts the kinematic range of the detected positrons to approximately $5 < E'_e < 20$ GeV and $Q^2 < 0.02$ GeV^2. The calculation of the geometric acceptance of the 35m tagger is complicated because the scattered positrons detected in the 35m tagger traverse the positron beampipe after passing through two bending magnets and three quadrupoles. Furthermore, scattered positrons have lower energy than the beam positrons and progressively leave the magnetic axis and are subject, in particular, to quadrupole fringe fields. Particular care, therefore, was taken to tune the beamline simulation before calculating this acceptance.

During normal HERA running, the positron-beam position and tilt at the interaction point vary over time. The positron-beam tilt may be monitored using the position of bremsstrahlung photons detected in the photon tagger. For this dedicated run, the beam position and tilt were controlled, carefully monitored and found to be very stable.

Bremsstrahlung data were taken immediately preceding the primary photoproduction data run to determine the effect, on the 35m-tagger bremsstrahlung acceptance, of variations in the positron-beam tilt and to tune beamline and detector simulations. From these data, the 35m-tagger acceptance was found to depend on the horizontal (X) tilt, but not significantly on the vertical (Y) tilt. The positron-energy interval of $12 < E'_e < 16$ GeV was chosen for the $\sigma_{\mathrm{tot}}^{\gamma p}$ measurement as the range least sensitive to variations of the positron-beam tilt. From this range of selected positron energies, the photon flux factor as determined from Eq.(4) is $f_\gamma = 0.004916$.

4 Event selection and background subtraction

Events were selected online by the three-level trigger system of ZEUS. The CAL is segmented into trigger towers [22] that are approximately projective; the towers consist of an EMC and a HAC part. In RCAL, the main component used in the CAL trigger, the EMC section of a typical trigger tower consists of two cells. The trigger required a measured energy deposit of more than 5 GeV in the 35m tagger in coincidence with a summed energy deposit in the RCAL EMC trigger towers of either more than 464 MeV (excluding the 8 towers immediately adjacent to the beampipe) or 1250 MeV (including those towers). In addition, the timing information from the CAL was required to be consistent with an ep collision.

The offline event-selection cuts on the 35m tagger and reconstructed RCAL energies were tighter than those applied at the trigger level. A positron energy in the range $12 < E'_e < 16$ GeV (see Section 3) was required in the 35m tagger. The energy requirement in the RCAL EMC section, summed over all cells above threshold, was: either more than 600 MeV (excluding the trigger

towers immediately adjacent to the beampipe); more than 1550 MeV (including those towers); or the sum of any two trigger towers was more than 850 MeV.

The CAL trigger-tower energies for every event were readout [23], permitting detailed trigger-efficiency studies. The offline energy thresholds were found to be well above the region of low-energy trigger inefficiencies, so that the resulting event selection was unaffected by the trigger cuts.

Positron-proton and positron-gas bremsstrahlung events in coincidence with RCAL energy deposition comprise the largest backgrounds in the online sample. Most of these background events were rejected offline by a cut on the photon-tagger energy, $E_\gamma < 1$ GeV. The residual $(1.26 \pm 0.26)\%$ positron-gas bremsstrahlung background in the sample was estimated using events associated with unpaired positron bunches, and was statistically subtracted from the photoproduction distributions used to calculate the cross section. The remaining number of events is $N = 22533 \pm 162$.

The background from proton-gas collisions, as measured using proton-only bunches, was found to be negligible. The final event sample was corrected for two background effects:

- a 0.99 ± 0.01 correction factor was applied to remove bremsstrahlung events which remained in the sample owing to the 97.0% acceptance of the photon tagger;
- a 1.043 ± 0.002 factor was applied to correct for photoproduction events lost due to overlays with bremsstrahlung events; the probability of overlay events was estimated using events triggered from random ep bunch crossings.

5 Simulation of photoproduction processes

The various physical processes that contribute to the hadronic total cross section are characterized by different distributions in energy and angle of the particles in the final state. To determine the acceptance of the CAL (see Section 6) for the various contributing processes, the simulation of the photoproduction sample was separated into the following subprocesses:

- elastic: $\gamma p \to Vp$, where V is one of the light vector mesons ρ^0, ω or ϕ;
- proton dissociative: $\gamma p \to VN$, where N is a hadronic state into which the proton diffractively dissociates;
- photon dissociative: $\gamma p \to Gp$, where G is a hadronic state into which the photon diffractively dissociates;
- double dissociative: $\gamma p \to GN$;
- hard non-diffractive: $\gamma p \to X$;
- soft non-diffractive: $\gamma p \to X$.

Process		A_{CAL}	Fraction
elastic	$\gamma p \to Vp$	0.477 ± 0.009	0.091
proton dissociative	$\gamma p \to VN$	0.531 ± 0.012	0.045
photon dissociative	$\gamma p \to Gp$	0.803 ± 0.006	0.133
double dissociative	$\gamma p \to GN$	0.824 ± 0.007	0.065
hard non-diffractive	$\gamma p \to X$	0.858 ± 0.005	0.166 ± 0.019
soft non-diffractive	$\gamma p \to X$	0.832 ± 0.003	0.498 ± 0.058

Table 1: CAL acceptance and fractions for the various photoproduction subprocesses for PYTHIA. Those fractions that have no listed uncertainty were fixed in the fitting procedure.

The first four processes are diffractive, in the sense that they can be parameterized at high energies in Regge theory by the exchange of a Pomeron trajectory. The hard non-diffractive part of photoproduction consists, in leading-order QCD, of direct and resolved photon components, which can be calculated perturbatively. The largest contribution to the cross section comes from the soft non-diffractive process. Two independent Monte Carlo (MC) samples were generated to simulate the various hadronic final states for photoproduction. The first sample was generated using PYTHIA 5.7 [24], with radiative corrections calculated by HERACLES 4.6 [25], and events from each of the subprocesses were selected separately. For the second sample, HERWIG 5.9 [26] was used for the non-diffractive reactions, while the diffractive processes were again generated with PYTHIA. Hard non-diffractive photoproduction events were simulated in both MC generators at leading order with parton showers, using CTEQ4L [27] and GRVG LO [28] for the proton and photon parton distributions, respectively; a minimum transverse momentum of the partonic hard scatter, $\hat{p}_T^{\min} = 2.5$ GeV, was used. These two samples were passed through the trigger and detector simulations and offline analysis.

6 Acceptance of the hadronic final state

To find the overall acceptance of the CAL, a weighted sum of the MC photoproduction subprocesses was simultaneously fitted to the invariant mass of the hadronic final state detected in the CAL, M_X^{CAL}, and the number of CAL cells, N_{cells}, in the data. The CAL acceptance for each subprocess was calculated as the fraction of generated events that pass the RCAL offline cuts; these individual acceptances are shown in Table 1. The overall acceptance of the CAL was then calculated using the fitted fraction and the acceptance for each subprocess. Because the data distributions were not described perfectly by the MC, the distribution of the soft non-diffractive subprocess, which is the MC process least constrained by experiment, was re-weighted. The re-weighting function was calculated separately for each of the following distributions: the pseudorapidity of the CAL cells, the total transverse energy and the RCAL energy.

To determine the subprocess fractions, the direct-to-resolved cross-section ratio was fixed to that used in the PYTHIA MC generator and factorization was assumed to estimate the double dissociative cross section by using

$$\frac{\sigma(\gamma p \to Vp)}{\sigma(\gamma p \to VN)} = \frac{\sigma(\gamma p \to Gp)}{\sigma(\gamma p \to GN)}.$$

The elastic ρ^0 [10], ω [11] and ϕ [12] cross sections, the elastic to proton-dissociative ratio [13], and the photon-dissociative fraction [14] were all fixed to values obtained from ZEUS measurements extrapolated to the $W_{\gamma p}$ of the present measurement. This reduced the fit parameters to two: the soft and hard non-diffractive fractions.

The data and fitted MC distributions of $M_X^{\rm CAL}$ and $N_{\rm cells}$ are shown in Figs. 1 and 2, respectively. The subprocess contributions are also shown. The detailed description of the systematic uncertainty calculation, shown as a band in the figures, is given in Section 9. As a consistency check, the RCAL energy distribution, which is not used in the fit, is shown in Fig. 3 with the MC distributions. In Fig. 4, a comparison of the data and MC distributions is shown for various CAL quantities. Overall, the data are well described by the fitted MC samples. The CAL acceptance is $A_{\rm CAL} = 0.781^{+0.022}_{-0.016}$(syst.). The largest contribution to the systematic uncertainty results from the different MC models used to calculate the acceptance and is discussed in Section 9.

7 Acceptance of the 35m tagger

The acceptance of the 35m tagger for scattered positrons was determined from a PYTHIA MC simulation of photoproduction. The bremsstrahlung data were used to determine the parameters of the incoming positron beam to be used in the BREMGE MC generator [29].

For the range of bremsstrahlung photon and positron energies relevant to the current measurement, bremsstrahlung photons were detected in the photon tagger and bremsstrahlung positrons in the 35m tagger with high efficiency. In particular, the photon-tagger acceptance for photons with energy greater than 1 GeV was 97.0%. The 35m-tagger acceptance for scattered bremsstrahlung positrons was defined to be the number of events containing a positron with $E'_e > 5$ GeV in the 35m tagger and a photon with energy $E_\gamma > 5$ GeV in the photon detector, divided by the total number of events containing a photon with energy $E_\gamma > 5$ GeV in the photon detector. Because the 35m-tagger bremsstrahlung acceptance was found to be sensitive primarily to variations in the horizontal plane, the MC alignment tuning was restricted to the X-vertex position and X tilt. Four distributions of both bremsstrahlung data and bremsstrahlung MC [29] events were used to form a χ^2, which was minimized with respect to the MC X-vertex position and X tilt: the photon energy; the positron energy; the 35m-tagger bremsstrahlung acceptance; and the average positron X position versus energy measurement. The bremsstrahlung data and MC distributions after tuning are shown in Fig. 5. There is good agreement between data and MC events except in Fig. 5c) for photon energies above $\sim$15 GeV. This region is not used in the current measurement.

The tuned values were used in the generation of PYTHIA MC samples and the 35m-tagger photoproduction acceptance was calculated. In Fig. 6, the measured and simulated energy spectra of the scattered positron are compared. Figure 7 shows the correlation between the scattered-positron position and energy, as measured with the 35m tagger, for the data and Monte Carlo simulation. The agreement between the data and the PYTHIA events is good. The resulting 35m-tagger photoproduction acceptance for $12 < E'_e < 16$ GeV is $A_{\rm 35m} = 0.693 \pm 0.050$(syst.).

8 Radiative corrections

The positron that initiates the γp interaction is subject to QED radiation in both the initial and final states. This changes the kinematics of the reaction and hence the measured cross section. The effect of QED radiation on the measurement can be greatly reduced by excluding hard initial-state bremsstrahlung. This was achieved by a veto on photons with energy larger than 1 GeV in the photon detector. The influence of radiation on the measured cross section can be described by a correction factor which is the ratio of the Born cross section to that including QED radiation.

The calculation of the correction factor was carried out with the HERACLES MC program that includes the positron-beam angular divergence at the interaction point. The result for the correction factor is 0.981 ± 0.007(syst.).

The systematic uncertainties on the correction factor were estimated from the range of values obtained for different parameterizations of the cross section, from a comparison with the analytic calculation of HECTOR 1.11 [30] and from varying the values of the photon-energy cut and angular acceptance within the experimental uncertainties.

9 Systematic uncertainty estimation

The systematic uncertainties in the $\sigma_{\rm tot}^{\gamma p}$ measurement come primarily from the uncertainties in the determination of the CAL and 35m-tagger acceptances.

The systematic uncertainty on the CAL acceptance was estimated by varying the CAL energy scale by $\pm 3\%$, leading to an effect of $^{+0.006}_{-0.008}$. The 35m-tagger energy scale was varied by $\pm 3\%$ and led to a small effect. The measured elastic cross sections [10–12], the fraction of the photon-dissociative processes [13], and the elastic to proton-dissociative cross-section ratio [14] were also varied by one standard deviation in the fitting procedure. The uncertainty due to the measured photon-dissociative cross section was $^{+0.008}_{-0.010}$; the others gave small effects. The uncertainty in modeling the non-diffractive hadronic final state was determined from a comparison of the PYTHIA and HERWIG MC simulations. This led to a $+0.019$ uncertainty. Several strategies were employed to fit the experimental distributions by varying the fractions of the processes shown in Table 1. A fit yielding the fractions of elastic, photon dissociation and hard and soft non-diffraction was performed. The resulting elastic and photon-dissociative fractions were found to be consistent with the ZEUS measurements, extrapolated to the $W_{\gamma p}$ of the present measurement. Global fits were made simultaneously to a number of experimental distributions or separately to individual distributions; the resulting systematic uncertainties on the CAL acceptance were negligible. Adding all of the above contributions in quadrature results in a CAL acceptance of $0.781^{+0.022}_{-0.016}$.

The sources of largest systematic uncertainty in the 35m-tagger acceptance are: the uncertainty in modeling the trajectories of the scattered positrons, i.e., the X-vertex position (± 0.027); the geometric description of the positron-beam angular spread (± 0.021); the details of the HERA beamline simulation (± 0.020); the uncertainty on the energy calibration of the photon detector

(± 0.015), and its energy nonlinearity (± 0.020). All of the contributions, of which the above are the most important, are added in quadrature and result in an uncertainty on the 35m-tagger acceptance of ± 0.050.

The 35m-tagger acceptance calculation was checked using an event sample containing two or more jets in the CAL, which was taken with a trigger independent of the 35m tagger. For these events, the inelasticity y can be determined from CAL energies only. The probability for these events to have a positron detected in the 35m tagger was compared to the probability determined from the tuned photoproduction MC simulation; the simulated events and data were consistent within the quoted systematic uncertainty.

10 Results

The measured photon-proton total cross section is given by

$$\sigma_{\rm tot}^{\gamma p} = \frac{N \cdot \Delta_{\rm corr}}{\mathcal{L} \cdot f_\gamma \cdot A_{\rm 35m} \cdot A_{\rm CAL}},$$

where N is the number of events passing the selection cuts (22533 ± 162), $\mathcal{L} =$ is the integrated luminosity (49.26 ± 0.54 nb^{-1}), f_γ is the photon flux factor (0.004916), $A_{\rm 35m}$ is the 35m-tagger acceptance (0.693 ± 0.050), and $A_{\rm CAL}$ is the CAL acceptance ($0.781^{+0.022}_{-0.016}$). The correction factor, $\Delta_{\rm corr}$, is the product of the radiative correction to the electroweak Born-level cross section (0.981 ± 0.007), the correction for bremsstrahlung background events in which the bremsstrahlung photon was lost due to the photon-tagger acceptance (0.99 ± 0.01), and the correction for photoproduction events lost due to an accidental overlay with bremsstrahlung events (1.043 ± 0.002). The 35m-tagger acceptance and CAL acceptance were assumed to be independent of each other. All acceptances and correction factors were calculated for the $195 < W_{\gamma p} < 225$ GeV range of this measurement.

The photoproduction total cross section, measured at the average photon-proton center-of-mass energy of 209 GeV, is

$$\sigma_{\rm tot}^{\gamma p} = 174 \pm 1({\rm stat.}) \pm 13({\rm syst.})\ \mu{\rm b}.$$

11 Discussion of results

The photon-proton total cross section as a function of the center-of-mass energy is shown in Fig. 8. The present result is in good agreement with a measurement from H1 [15] at a similar center-of-mass energy and is consistent with the previous ZEUS measurements [9], which it supersedes. The low-energy data [8] are also shown in Fig. 8. The present result can also be compared with an earlier ZEUS measurement [31] of the inclusive electroproduction cross section in the range $0.11 \leq Q^2 \leq 0.65\,{\rm GeV}^2$. Extrapolating the cross section to $Q^2 = 0$, using the generalized VDM, yields the photoproduction total cross section. This is much more model dependent and leads to a cross section of $187 \pm 5({\rm stat.}) \pm 14({\rm syst.})$ μb at a center-of-mass energy of $W_{\gamma p} = 212$ GeV, in agreement within errors with the present measurement.

Fits of hadronic total cross sections and an investigation of their universal high-energy behavior have been carried out by Donnachie and Landshoff [2] using the form of Eq. (1). A similar fit has been performed by Cudell *et al.* [3] based on more recent hadronic data. A ZEUS fit of the form

$$\sigma_{tot} = A \cdot W_{\gamma p}^{2\epsilon} + B \cdot W_{\gamma p}^{-2\eta}, \tag{5}$$

where $W_{\gamma p}$ is in GeV, to the existing γp data [8,15] and including the present measurement has been performed and is shown as the solid curve in Fig. 8. The present fit has been restricted to $W_{\gamma p} > 4$ GeV and the Reggeon intercept ($\alpha_{I\!R}(0) = 1 - \eta$) has been fixed to the value found by Cudell *et al.*, $\eta = 0.358 \pm 0.015$. The resulting fit parameters are:

$$A = 57 \pm 5\,\mu\text{b};\ B = 121 \pm 13\,\mu\text{b};\ \epsilon = 0.100 \pm 0.012\,. \tag{6}$$

The resulting value of ϵ, related to the Pomeron intercept ($\alpha_{I\!P}(0) = 1 + \epsilon$), is in good agreement with $\epsilon = 0.093 \pm 0.002$ found by Cudell *et al.*, a value derived primarily from pp and $\bar{p}p$ data.

A fit including a soft- and hard-Pomeron trajectory by Donnachie and Landshoff (DL98) [4] also agrees with the present measurement within uncertainties, as shown by the dot-dashed curve in Fig. 8. Other models [5, 32] based on the existing hadron-hadron total cross-section data are also in agreement with this measurement.

The optical theorem and VDM provide a connection between the photon-proton total cross section and the forward elastic scattering amplitudes for photoproduction of vector-meson states, V, via

$$\sigma_{\text{tot}}^{\gamma p} = \sqrt{16\pi \cdot \left.\frac{d\sigma^{\gamma p \to \gamma p}}{dt}\right|_{t=0}} = \sum_{V=\rho^0,\omega,\phi} \sqrt{16\pi \cdot \frac{4\pi\alpha}{f_V^2} \cdot \left.\frac{d\sigma^{\gamma p \to V p}}{dt}\right|_{t=0}}\,.$$

The forward elastic scattering amplitudes for the $\gamma p \to \gamma p$ and $\gamma p \to V p$ cross sections have been assumed to be purely imaginary and f_V are the photon to vector-meson coupling constants.

Summing only over the light vector-meson states ρ^0, ω and ϕ, using the exclusive photoproduction differential cross sections from ZEUS measurements [10–12], and values of $f_V^2/4\pi = 2.20$, 23.6 and 18.4 [7] for ρ^0, ω and ϕ, respectively, a value of $111 \pm 13(\text{exp.})\,\mu$b is obtained for the photon-proton total cross section at $W_{\gamma p} = 70$ GeV. The ρ^0 meson contributes about 85% of this value. The photon-proton total cross section at a center-of-mass energy of $W_{\gamma p} = 70$ GeV, obtained by interpolation between the present measurement and the lower energy measurements using the fit described by Eqs. (5) and (6), is 139 ± 4 μb. Given the additional theoretical uncertainties in the VDM calculation of 111 μb, these results are consistent.

The present measurement can also be used to test factorization, which connects $\gamma\gamma$, γp and pp total cross sections according to

$$\sigma_{\text{tot}}^{\gamma\gamma} \cdot \sigma_{\text{tot}}^{pp} = (\sigma_{\text{tot}}^{\gamma p})^2\,. \tag{7}$$

The $\gamma\gamma$ total cross section has been measured at high energies by the OPAL [33] and L3 [34] collaborations. Using Eq. (7) at the energy of the OPAL and L3 measurements requires an interpolation from the present measurement to lower center-of-mass energies. Using the fit described by Eqs. (5) and (6) and the Cudell *et al.* parameterization of the pp total cross

sections, a value $\sigma_{\rm tot}^{\gamma\gamma} = 436 \pm 28$ nb (468 ± 30 nb) is obtained for a center-of-mass energy of 68 (95) GeV, in agreement with the OPAL measurement of 439^{+45}_{-41} (464^{+76}_{-62}) nb at those energies. Measurements from L3 agree within uncertainties with those from OPAL for $W_{\gamma\gamma} < 100$ GeV. Thus the present $\sigma_{\rm tot}^{\gamma p}$ measurement is consistent with the factorization hypothesis of Eq. (7).

At $W_{\gamma\gamma} = 120.4$ GeV, L3 [34] finds 572.0 ± 3.3(stat.) ± 53(exp. syst.) ± 89(MC syst.) nb, while at an energy of 158.7 GeV, they find 734.1 ± 8.7(stat.) ± 102(exp. syst.) ± 202(MC syst.) nb. There is an additional uncertainty of $\pm 5\%$ due to the luminosity measurement. Interpolations from the present $\sigma_{\rm tot}^{\gamma p}$ measurement give 491 ± 35 nb and 521 ± 43 nb, respectively. Within the large systematic uncertainties of the L3 measurement, these data are also consistent with factorization.

In earlier parameterizations [2–5], the high-energy dependence has effectively been determined from the pp and $\bar{p}p$ data. The compatibility of the current ZEUS $\sigma_{\rm tot}^{\gamma p}$ measurement with this high-energy behavior indicates a universality of the energy dependence of the photon-proton total cross section with respect to that of hadron-proton total cross sections.

Acknowledgements

We thank the DESY directorate for their strong support and encouragement. The special efforts of the HERA machine group in the collection of the data used in this paper are gratefully acknowledged. We thank the DESY computing and network services for their support. The design, construction and installation of the ZEUS detector have been made possible by the ingenuity and effort of many people from DESY and home institutes who are not listed as authors. We are grateful for the helpful discussions and correspondence with A. Arbuzov, D. Bardin, M. Block, H. Spiesberger and T. Sjöstrand.

References

[1] P.D.B. Collins, *An Introduction to Regge Theory and High Energy Physics*, Cambridge University Press (1977).

[2] A. Donnachie and P.V. Landshoff, Phys. Lett. **B296**, 227 (1992).

[3] J.R. Cudell *et al.*, Phys. Rev. **D61**, 034019 (2000), Erratum-ibid. **D63**, 059901 (2001).

[4] A. Donnachie and P.V. Landshoff, Phys. Lett. **B437**, 408 (1998).

[5] C. Friberg and T. Sjöstrand, JHEP **09**, 010 (2000), and references therein.

[6] J.J. Sakurai, Ann. Phys. (NY) **11**, 1 (1960);
J.J. Sakurai, Phys. Rev. Lett. **22**, 981 (1969).

[7] T.H. Bauer *et al.*, Rev. Mod. Phys. **50**, 261 (1978), Erratum-ibid. **51**, 407 (1979).

[8] D.O. Caldwell *et al.*, Phys. Rev. Lett. **40**, 1222 (1978);
S.I. Alekhin *et al.*, CERN Report HERA 87-01 (1987).

[9] ZEUS Collab., M. Derrick *et al.*, Phys. Lett. **B293**, 465 (1992);
ZEUS Collab., M. Derrick *et al.*, Z. Phys. **C63**, 391 (1994).

[10] ZEUS Collab., M. Derrick *et al.*, Z. Phys. **C69**, 39 (1995).

[11] ZEUS Collab., M. Derrick *et al.*, Z. Phys. **C73**, 73 (1996).

[12] ZEUS Collab., M. Derrick *et al.*, Phys. Lett. **B377**, 259 (1996).

[13] ZEUS Collab., J. Breitweg *et al.*, Eur. Phys. J. **C2**, 247 (1998);
K. Desler, Ph.D. Thesis, Universität Hamburg (2000), (unpublished).

[14] ZEUS Collab., J. Breitweg *et al.*, Z. Phys. **C75**, 421 (1997).

[15] H1 Collab., S. Aid *et al.*, Z. Phys. **C69**, 27 (1995).

[16] V.N. Gribov *et al.*, Sov. Phys. JETP **14**, 1308 (1962).

[17] B. Badełek, J. Kwieciński, and A. Staśto, Z. Phys. **C74**, 297 (1997);
D. Schildknecht and H. Spiesberger, BI-TP 97/25, *hep-ph/9707447*;
D. Schildknecht, Acta Phys. Polon. **B28**, 2453 (1997).

[18] ZEUS Collab., U. Holm (ed.), *The ZEUS Detector,* Status Report, (unpublished), DESY, 1993;
`http://www-zeus.desy.de/bluebook/bluebook.html` .

[19] M. Derrick *et al.*, Nucl. Instr. and Meth. **A309**, 77 (1991);
A. Andresen *et al.*, Nucl. Instr. and Meth. **A309**, 101 (1991);
A. Caldwell *et al.*, Nucl. Instr. and Meth. **A321**, 356 (1992);
A. Bernstein *et al.*, Nucl. Instr. and Meth. **A336**, 23 (1993).

[20] N. Harnew *et al.*, Nucl. Instr. and Meth. **A279**, 290 (1989);
B. Foster *et al.*, Nucl. Phys. Proc. Suppl. **B32**, 181 (1993);
B. Foster *et al.*, Nucl. Instr. and Meth. **A338**, 254 (1994).

[21] D. Kisielewska *et al.*, Nukleonika **31**, 205 (1986);
J. Andruszków *et al.*, DESY Report 92-066 (1992);
J. Andruszków *et al.*, DESY Report 01-041 (2001).

[22] W.H. Smith *et al.*, Nucl. Instr. and Meth. **A355**, 278 (1995).

[23] B.G. Bylsma *et al.*, Nucl. Instr. and Meth. **A337**, 512 (1994).

[24] T. Sjöstrand, PYTHIA 5.7, *hep-ph/9508391*;
T. Sjöstrand, Comp. Phys. Comm. **82**, 74 (1994).

[25] A. Kwiatkowski, H. Spiesberger and H.-J. Möhring, Comp. Phys. Comm. **69**, 155 (1992);
H. Spiesberger, HERACLES 4.6 Manual, `http://www.desy.de/~hspiesb/heracles.html` .

[26] G. Marchesini *et al.*, HERWIG 5.9, *hep-ph/9607393*;
G. Marchesini *et al.*, Comp. Phys. Comm. **67**, 465 (1992).

[27] CTEQ Collab., H.L. Lai *et al.*, Phys. Rev. **D55**, 1280 (1997).

[28] M. Glück, E. Reya and A. Vogt, Phys. Rev. **D45**, 3986 (1992);
M. Glück, E. Reya and A. Vogt, Phys. Rev. **D46**, 1973 (1992).

[29] K. Piotrzkowski and L. Suszycki, *Proceedings of the Workshop on Physics at HERA, Oct. 1991*, Volume 3, W. Buchmüller and G. Ingelman (eds.), DESY (1992), p. 1463.

[30] A. Arbuzov *et al.*, Comp. Phys. Comm. **94**, 128 (1996);
A. Arbuzov *et al.*, Hector 1.00 Manual, DESY Report 95-185, *hep-ph/9511434*.

[31] ZEUS Collab., J. Breitweg *et al.*, Eur. Phys. J. **C7**, 609 (1999).

[32] M.M. Block *et al.*, Phys. Rev. **D60**, 054024 (1999);
M.M. Block, F. Halzen and T. Stanev, Phys. Rev. **D62**, 077501 (2000).

[33] OPAL Collab., G. Abbiendi *et al.*, Eur. Phys. J. **C14**, 199 (2000).

[34] L3 Collab., M. Acciarri *et al.*, Phys. Lett. **B519**, 33 (2001).

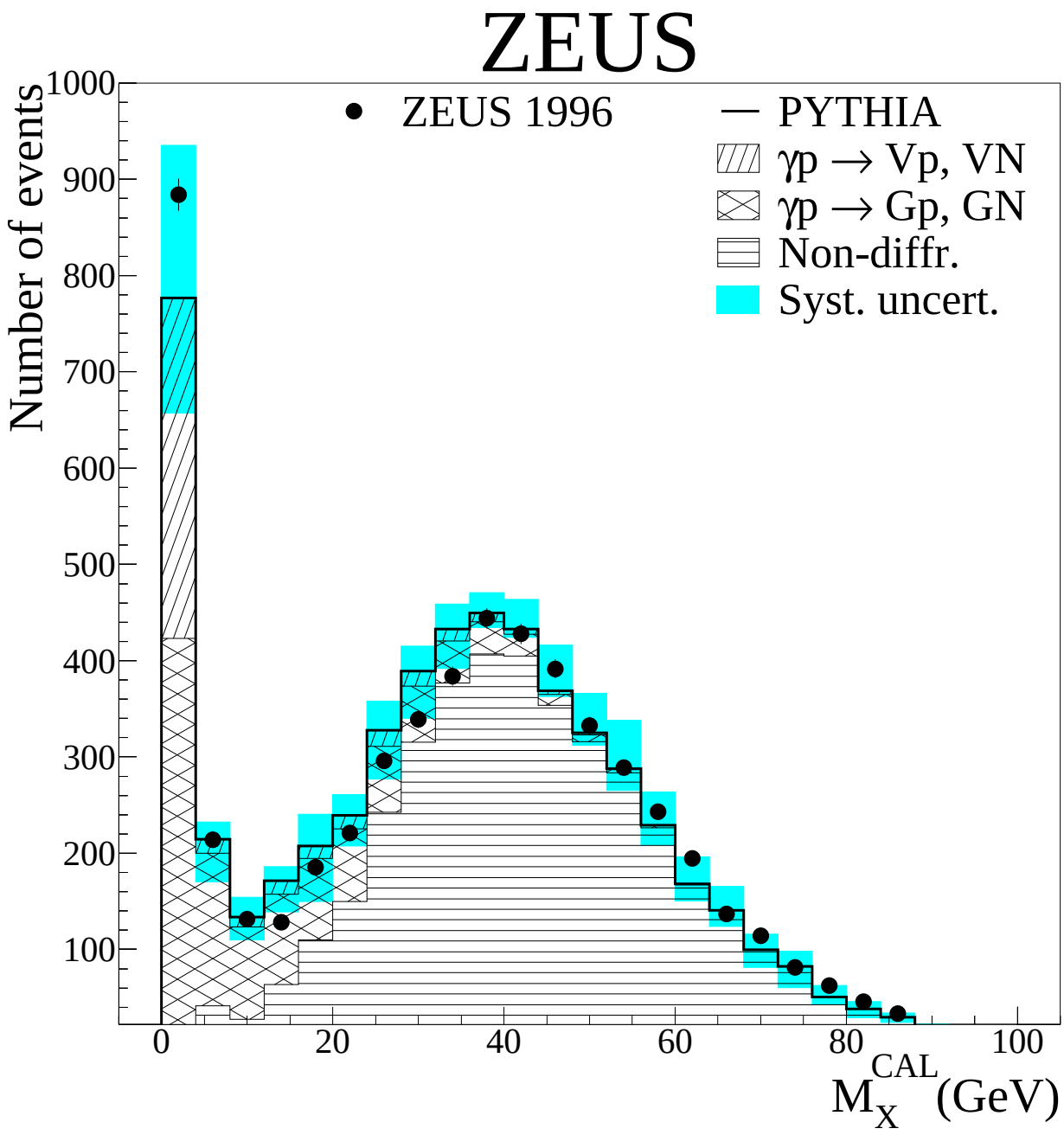

Figure 1: M_X^{CAL} distribution for data (filled circles) and fitted total photoproduction MC sample (histogram with systematic uncertainty band). The fit is made to the M_X^{CAL} and N_{cells} distributions. Cumulative subprocess contributions are also shown. The elastic and proton-dissociative samples have been combined, as have the photon-dissociative and double-dissociative samples and the soft and hard non-diffractive samples.

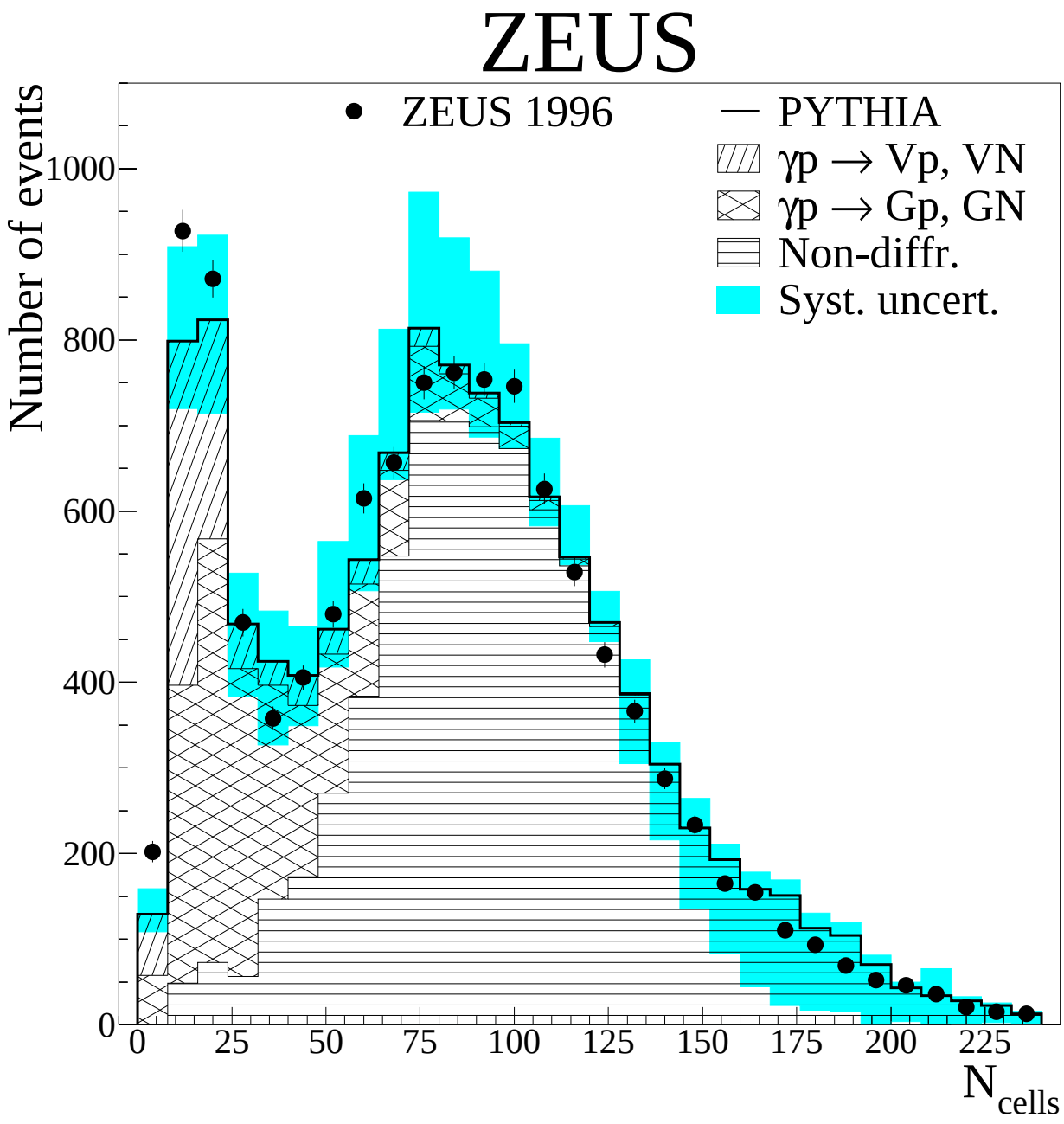

Figure 2: $N_{\rm cells}$ distribution for data (filled circles) and fitted total photoproduction MC sample (histogram with systematic uncertainty band). The fit is made to the $M_X^{\rm CAL}$ and $N_{\rm cells}$ distributions. Cumulative subprocess contributions are also shown. The elastic and proton-dissociative samples have been combined, as have the photon-dissociative and double-dissociative samples and the soft and hard non-diffractive samples.

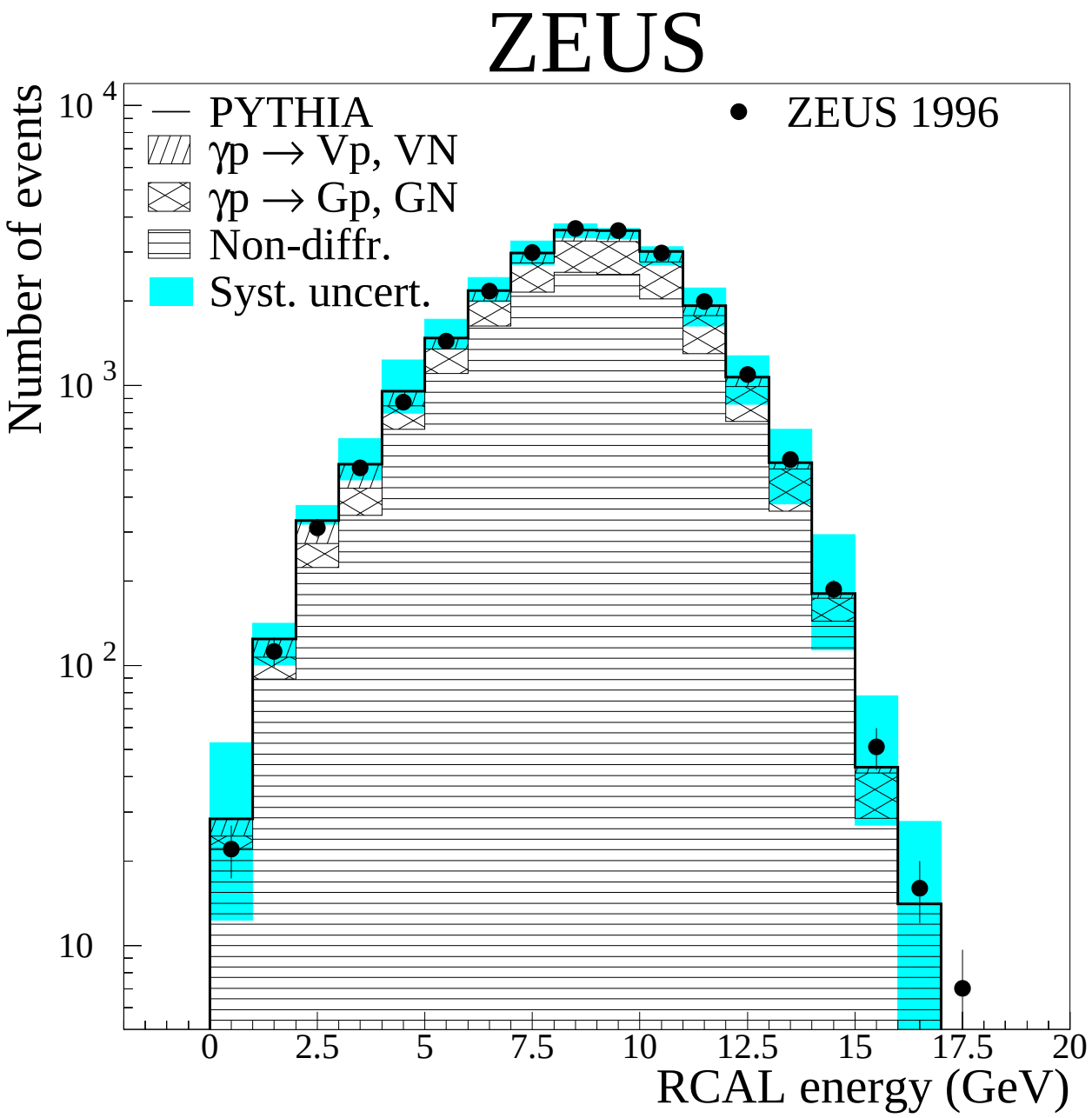

Figure 3: RCAL energy distribution for data (filled circles) and fitted total photoproduction MC sample (histogram with systematic uncertainty band). The fit is made to the M_X^{CAL} and N_{cells} distributions. Cumulative subprocess contributions are also shown. The elastic and proton-dissociative samples have been combined, as have the photon-dissociative and double-dissociative samples and the soft and hard non-diffractive samples.

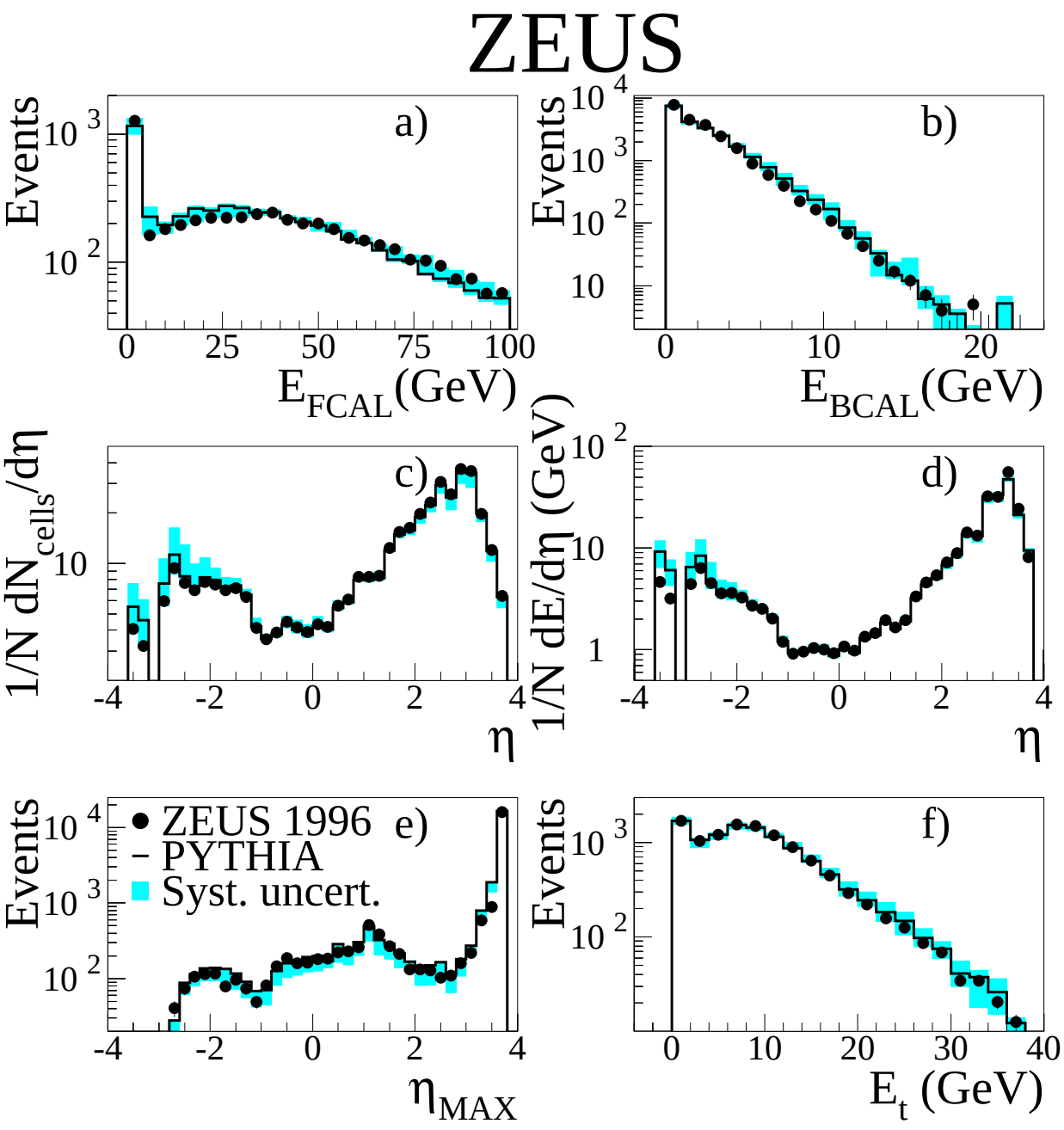

Figure 4: Comparison of the data (filled circles) and fitted photoproduction MC sample (histogram with systematic uncertainty band) for a) FCAL energy, b) BCAL energy, c) pseudorapidity of the CAL cells, d) energy-weighted pseudorapidity of the CAL cells, e) pseudorapidity of the most forward energy deposit of those CAL EMC cells above 80 MeV or the CAL HAC cells above 140 MeV and f) total transverse energy of each event. The fit is made to the $M_X^{\rm CAL}$ and $N_{\rm cells}$ distributions.

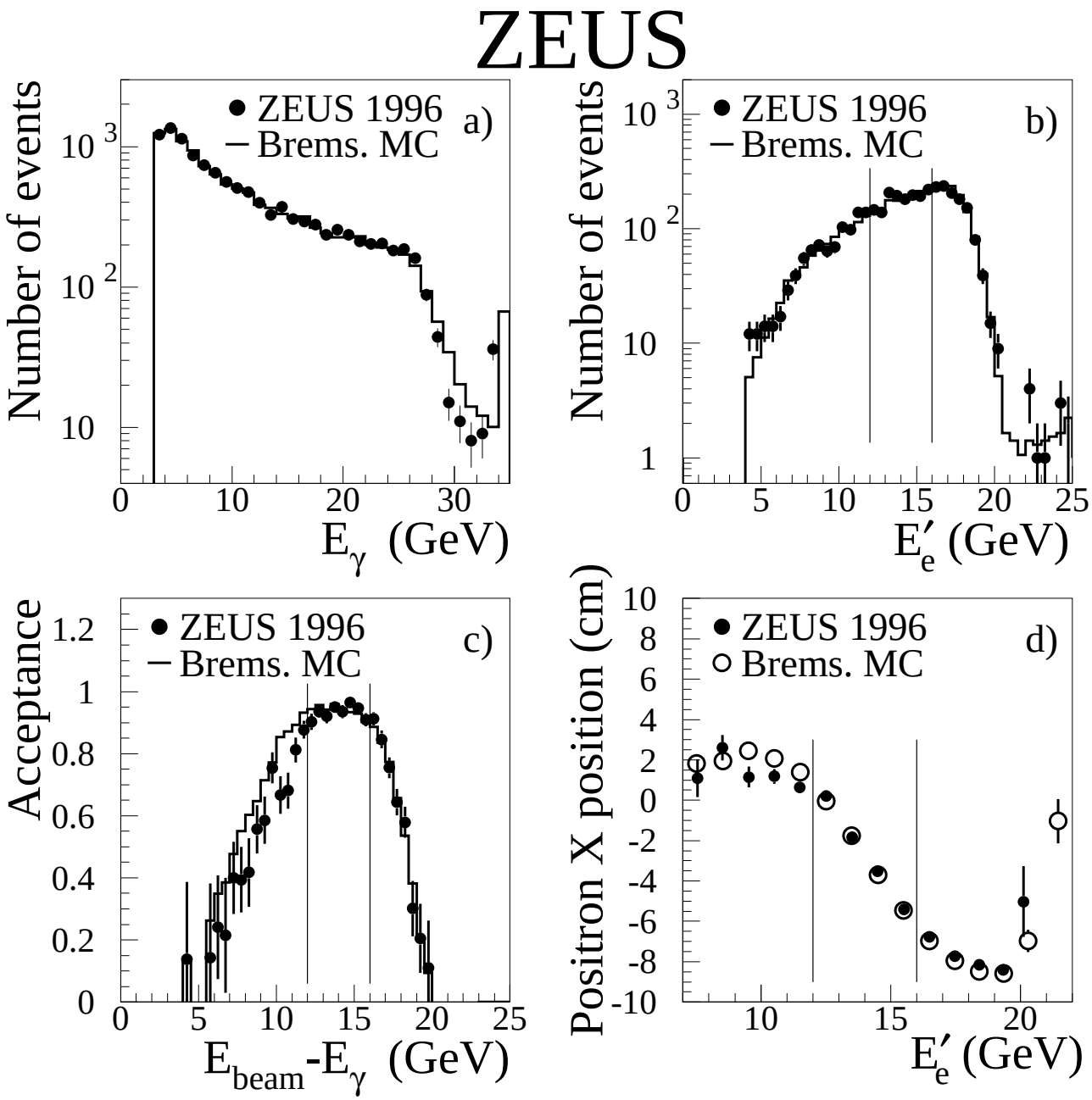

Figure 5: Distributions for the bremsstrahlung data (filled circles): a) photon energy, b) positron energy, c) 35m-tagger bremsstrahlung acceptance as a function of the predicted positron energy and d) positron position vs. positron energy. In (b-d), the region used for the scattered positron energy in the $\sigma_{\rm tot}^{\gamma p}$ measurement, $12 < E'_e < 16$ GeV, is shown by the vertical lines. The tuned bremsstrahlung Monte Carlo simulation is shown in (a-c) as the histogram and in d) as the open circles.

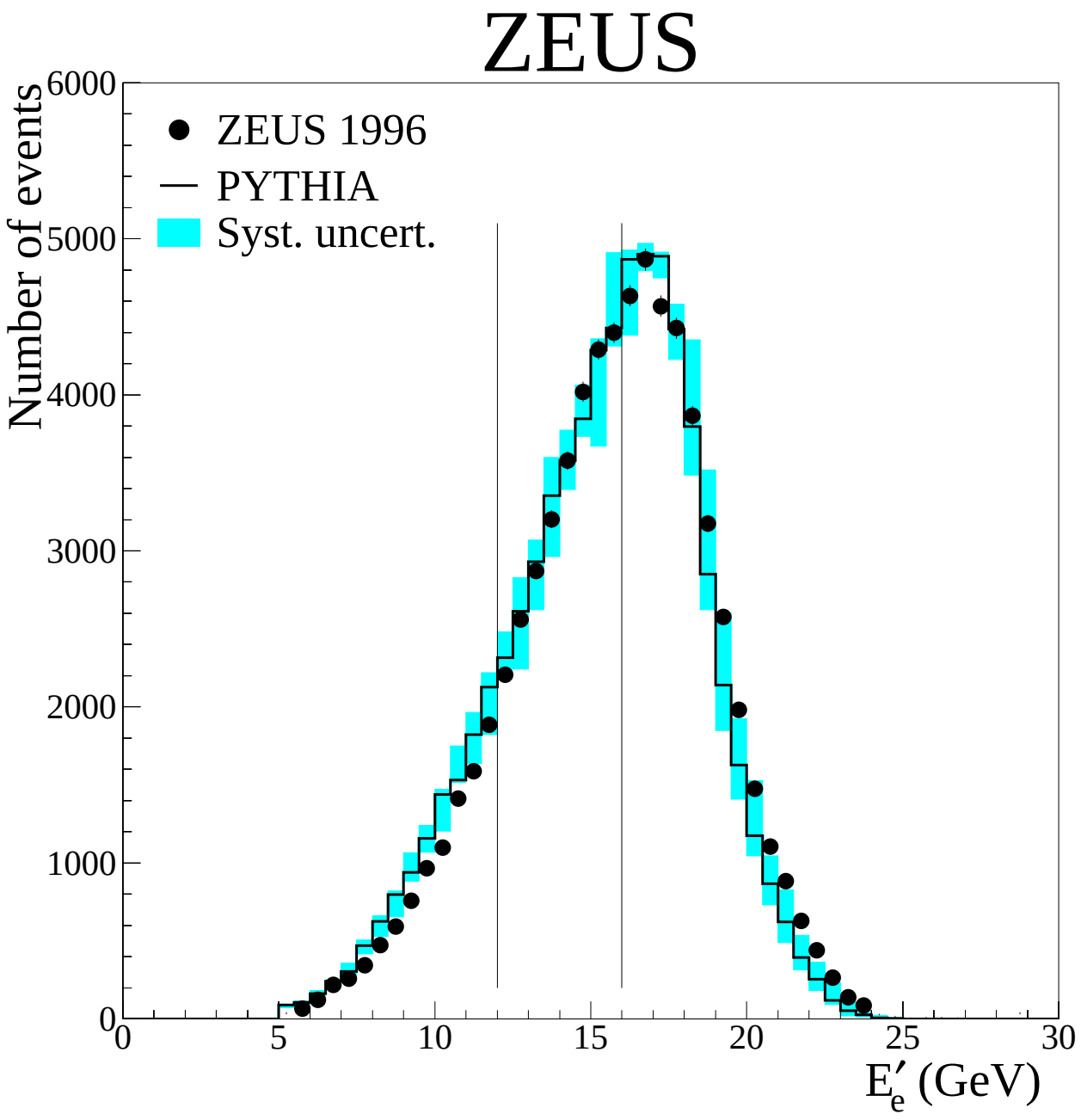

Figure 6: The positron energy distribution for photoproduction data (filled circles) and tuned MC events (histogram with systematic uncertainty band). The selected region, $12 < E'_e < 16$ GeV, is shown by the vertical lines.

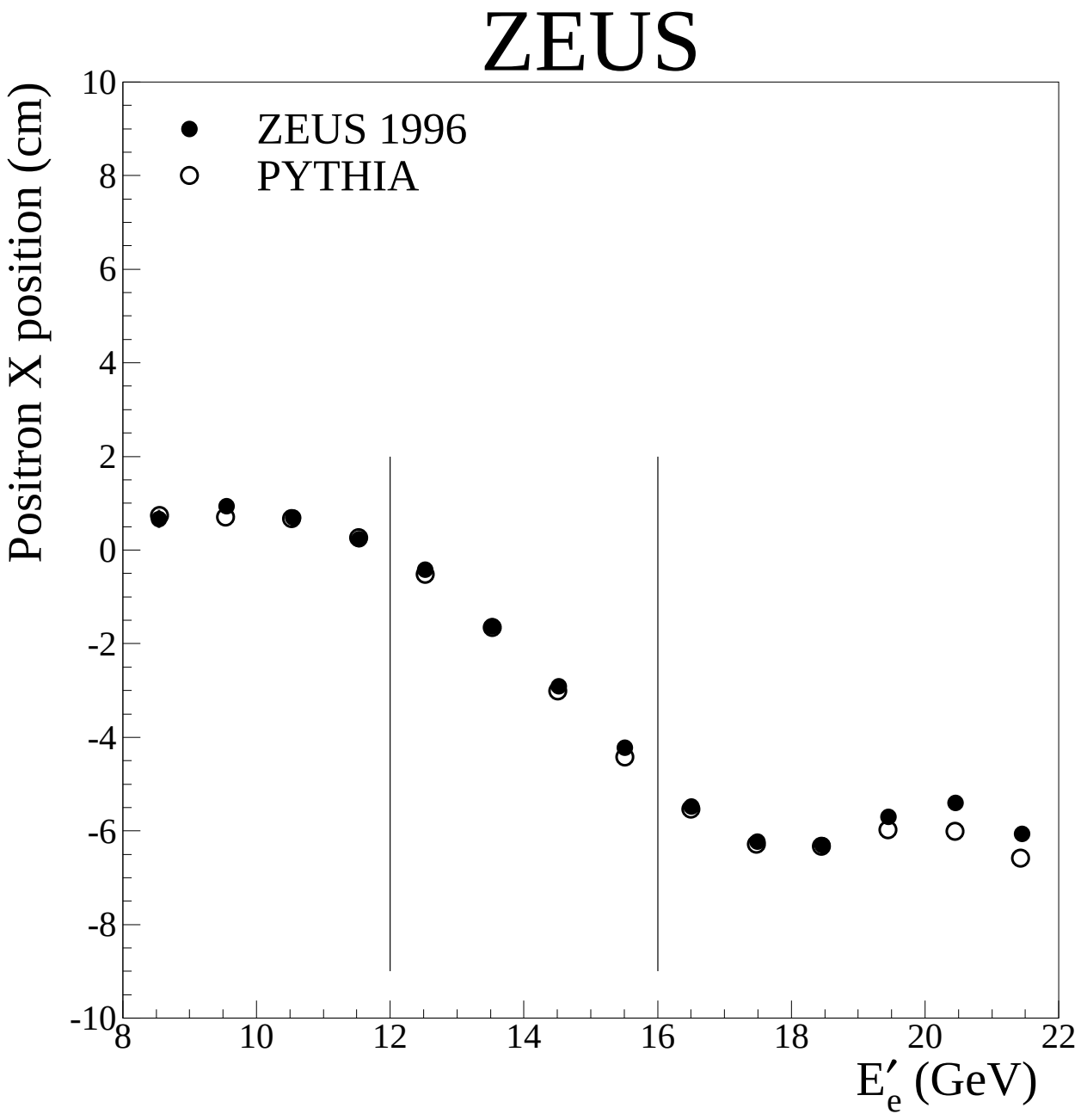

Figure 7: The correlation between the position and energy of the scattered positrons for photoproduction data (filled circles) and MC events after tuning of the X tilt and X position (open circles). The selected region, $12 < E'_e < 16$ GeV, is shown by the vertical lines.

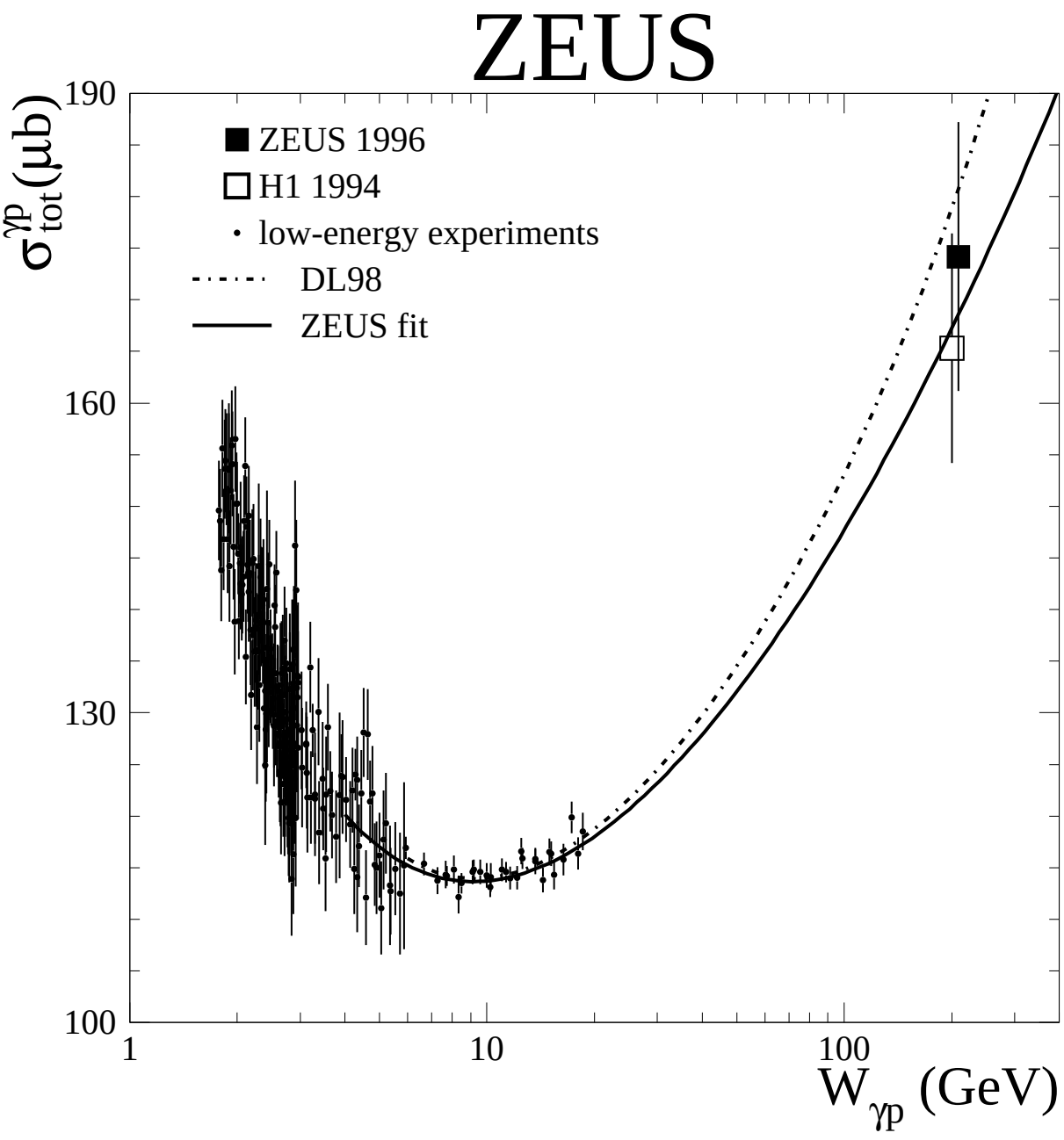

Figure 8: The photon-proton total cross section as a function of photon-proton center-of-mass energy. The present measurement is shown as the filled square. Also shown are the published H1 value (open square), the low-energy data (filled circles), the DL98 parameterization (dot-dashed curve) and the ZEUS fit (solid curve) described by Eqs. (5) and (6), see text.